Available online at www.sciencedirect.com
SCIENCE DIRECT®
Combustion and Flame 139 (2004) 279–287
Combustion and Flame
www.elsevier.com/locate/jnlabr/cnf

Modeling of soot particle inception in aromatic and aliphatic premixed flames

Angela Violi

Department of Chemical Engineering, University of Utah, Salt Sake City, UT 84112, USA
Department of Chemistry, University of Utah, Salt Sake City, UT 84112, USA

Received 6 August 2003; received in revised form 20 July 2004; accepted 20 August 2004

Available online 13 October 2004

Abstract

The growth of hydrocarbon molecules up to sizes of incipient soot is computed in premixed laminar flames using kinetic Monte Carlo and molecular dynamic methodologies (AMPI code). This approach is designed to preserve atomistic scale structure (bonds, bond angles, dihedral angles) as soot precursors evolve into three-dimensional structures. Application of this code to aliphatic (acetylene) and aromatic (benzene) flame environments is able to explain results in the literature on the differences in properties of soot precursors from these two classes of flames, particularly relating to H/C ratio, particle sphericity, and depolarization ratio.

Keywords: Molecular dynamics; Kinetic Monte Carlo; Soot inception

1. Introduction

Within the soot formation process, the transition from gas-phase compounds to nascent isolated spherules represents a dramatic change in both chemical and physical properties [1]. The precursor particles thus formed have a liquid-like character, a composition typical of hydrocarbon tars, a presumed density around 1.2 g/mL, and a C/H ratio of about 2. They are optically transparent in the visible light spectrum and thus have a low imaginary component of the refractive index. The processes involved in the formation of soot precursors exhibit a wide range of time scales, spanning pico- or nanoseconds for intramolecular processes that can occur, for example, on a particle surface to milliseconds for intermolecular reactions. To accurately model the reactions occurring at different time scales, we use an approach that combines two atomistic methodologies: molecular dynamics (MD) and kinetic Monte Carlo (KMC).

The code named AMPI (atomistic model for particle inception) places the two simulation procedures on an equal footing and alternates between KMC and MD steps during the simulation. The use of this approach permits us to follow the growth of aromatic compounds up to the nanosize range in a chemically specific way. It is designed to preserve atomistic scale structure, such as bonds, bond angles, and dihedral angles. Some preliminary results have been reported in earlier publications on the evolution of soot precursors in premixed laminar flames [2,3].

To help resolve issues such as identification of pathways leading to soot formation, it is important to characterize the precursors in terms of chemical structure/components. Studying relationships between structure and pathways, structure and proper-

E-mail address: violi@eng.utah.edu.

0010-2180/$ – see front matter
doi:10.1016/j.combustflame.2004.08.013

ties, and structure and reactivity (population of active sites) may lead to a deeper understanding of soot growth mechanisms. We want to address these issues theoretically by studying the growth of molecules in combustion environments, using atomistic models.

In this article the AMPI code is used to study the growth of aromatic nanoparticles in aromatic and aliphatic laminar flames. The aromatic growth process strongly depends on the specific local environment, which is characterized by several experimentally measured properties, such as temperature, concentration of hydrogen, and polycyclic aromatic hydrocarbons (PAHs), and this work reveals the influence of different environments on structural properties of the compounds formed.

After summarizing in the following section the methodological details of the computations performed, we report an analysis of the reaction rates used in the code, and discuss the results of the molecular growth process in two different environments representative of low-pressure benzene and acetylene flames.

2. The AMPI code

Among atomistic simulations the most direct technique is the MD method, in which an appropriate interatomic potential is chosen to describe the forces between atoms, followed by an integration of the classic equation of motion with appropriate boundary conditions. An appealing feature of MD is that it follows the actual dynamical evolution of the system. However, the limitation in the accessible simulation time is a substantial obstacle in making useful predictions with MD. To solve this time scale problem, the MD methodology has been coupled to KMC to allow the extension of the accessible time scale by orders of magnitude relative to direct MD, while retaining full atomistic detail.

In a typical simulation, an aromatic seed molecule is placed in a combustion environment defined by temperature and concentrations of the species present in the gas phase that can contribute to the growth process. A list of all the possible events, i.e., reactions, is also provided to the code. During the KMC step [4–6] one reaction is executed at one site on the growing aromatic structure during each time step. The probability of choosing a reaction is equal to the rate at which the reaction occurs relative to the sum of the rates of all of the possible reactions. To choose one reaction, a list is constructed that contains a running sum of the rates of each of the possible events, and each entry in the list is normalized by the sum of the rates of all the possible events. At each time step, one event denoted by m is randomly chosen from all of the M events that can possibly occur at that step, as follows:

$$\frac{\sum_{i=0}^{m-1} r_i}{\sum_{i=0}^{M} r_i} < \zeta_1 < \frac{\sum_{i=0}^{m} r_i}{\sum_{i=0}^{M} r_i}. \tag{1}$$

Here r_i is the rate at which the event i occurs, and ζ_1 is a random number in the range $(0, 1)$. Once a reaction is chosen, the molecular system is altered appropriately and the list of relative rates is updated to reflect the new configuration. Since one event occurs at each simulation step and different events occur at different rates, the time increment, dt, associated with each simulation step is dynamic and stochastic,

$$dt = -\frac{\ln(\zeta_2)}{\sum_{i=1}^{M} r_i}, \tag{2}$$

where ζ_2 is a random number uniformly distributed in the range $(0, 1)$, and the denominator is the sum of the rates of all of the events that can occur at the simulation step for which dt has been evaluated [7]. The use of variable time increment allows the consideration of reactions that occur on widely disparate time scales.

The MD module is used to equilibrate the structures produced after the KMC steps, and the output is a phase space at equilibrium. The computations alternate between the KMC and MD components. The time between Monte Carlo events can be arbitrarily long (depending on the kinetics, model, etc.), whereas in MD, we require time steps that are a small fraction of a vibrational period. So the combination of the two techniques spans two time and equilibrium scales.

A first version of this code was applied to the formation of soot precursors in premixed laminar flames [2,8]. That version has been significantly modified [3] and the new code, named AMPI, has been used in this article. The potential used for these calculations is the adaptive intermolecular REBO potential known as AIREBO [9]. The extensions include an adaptive treatment of the nonbonded and dihedral angle interactions, which still allows for covalent bonding interactions. Torsional potentials are introduced via a novel interaction potential that does not require a fixed hybridization state. For carbon or hydrocarbon systems in which chemical reactions are of interest, and which require nonbonded interactions to be treated, the AIREBO potential provides an effective and accurate method of performing molecular simulations. The individual atomic velocities in the system are periodically resampled from the Boltzmann distribution at the given temperature so that the entire MD system is described within a weak collision model. The temperature resampling allows the user to equilibrate the system to a specified temperature. The atoms are randomly picked throughout the molecule at a user-defined collision rate.

The definition of sites where reactions can occur includes atoms on five- and six-membered rings, dangling bonds on five- and six-membered rings, sp^3 hydrogen, chains prone to close to form five-membered rings (HCCCCCH, HCCCCC*) and six-membered rings (HCCCCCCH, HCCCCCC*) [2], sites on generic aliphatic chains, and rings containing a number of carbons different from 5 or 6. Thirty species that describe the gas-phase environment are included (see Section 2.1.2), together with the corresponding rates. Microscopic reversibility and fragmentation reactions, where a radical breaks apart to form either a stable species and a radical or two radicals, were also included in the AMPI code.

Table 1 reports the main rates used for these calculations, together with their references.

2.1. Inputs to the code

The main inputs to the AMPI code are the temperature, concentrations of the species that can contribute to the growth, rate constants for the principal reactions that these species can undergo with the growing seed, and intramolecular reactions such as dehydrogenation.

2.1.1. Reaction rates

In this article we consider two main reaction sequences as possible pathways that can contribute to the aromatic growth. The first one was introduced by D'Anna and Violi [10], and it is based on the formation of resonantly stabilized structures of the reacting radicals, which follows the idea that hydrocarbons with conjugated structures and their derivatives are critical intermediates to soot nucleation [11]. Growth of aromatic compounds beyond three-ring PAHs is modeled by a radical-molecule sequence of reactions involving five-membered ring compounds, such as acenaphthylene, given by the sequence

R1: $\mathrm{R}_i\text{–H} + \mathrm{H} = \mathrm{R}_i + \mathrm{H}_2$,

R2: $\mathrm{R}_i + \mathrm{R}_j\text{–H} + \mathrm{H} = \mathrm{R}_i\mathrm{R}_j + \mathrm{H}_2$,

where R_i–H is an aromatic molecule with i pericondensed rings, and R_i is its radical.

The initiation step (R1) is represented by H abstraction reactions, which activate the aromatic structures. This can be accomplished in many different ways, but under conditions of typical flame and shock-tube experiments, H abstraction by gaseous H atoms typically dominates [12–14]. Aromatic radicals (R_i) then add to the conjugated double bond of five-membered PAHs (R_j–H) leading to $\mathrm{R}_i\mathrm{R}_j$. The product continues to grow by the same process until termination reactions occur. Termination reactions include the coupling of two growing radical intermediates and/or H atom addition to a radical. A detailed analysis of this sequence is reported elsewhere [15].

The second reaction sequence considered in this study is the HACA mechanism. The term HACA was introduced by Frenklach and Wang [16], as an acronym for H abstraction–$\mathrm{C}_2\mathrm{H}_2$ addition. This implies a repetitive reaction sequence of two principal steps: abstraction of hydrogen by H atom from hydrocarbons, which activates the aromatic molecules (R1), and

R3: $\mathrm{R}_i + \mathrm{C}_2\mathrm{H}_2 = \text{products}$

addition of acetylene to the radical site formed, which allows for molecular growth and cyclization of PAH. The rates used in the AMPI code for this sequence are those reported by Richter et al. in their theoretical study of acetylene addition to phenyl and 1-naphthyl radicals [17].

2.1.2. Gas-phase species

The other main inputs to the AMPI code are the concentrations of the species present in the gas phase that can contribute to the aromatic growth process. H, H_2, CH_4, CH_3, $\mathrm{C}_2\mathrm{H}_2$, $\mathrm{C}_2\mathrm{H}$, $\mathrm{C}_2\mathrm{H}_3$, $\mathrm{C}_2\mathrm{H}_4$, $\mathrm{C}_2\mathrm{H}_5$, $\mathrm{C}_3\mathrm{H}_3$, i-$\mathrm{C}_4\mathrm{H}_3$, i-$\mathrm{C}_4\mathrm{H}_5$, $\mathrm{C}_5\mathrm{H}_6$, $\mathrm{C}_5\mathrm{H}_5$, phenylacetylene, styrene, $\mathrm{C}_6\mathrm{H}_6$, $\mathrm{C}_6\mathrm{H}_5$, naphthalene, 1- and 2-naphthyl radicals, ethynylnaphthalene, acenaphthylene, 1-, 3-, 4-, and 5-acenaphthyl radicals, biphenyl, indene, and indenyl radical are considered in this work as key contributors to the PAH growth process and are used as inputs to the atomistic model.

A low-pressure benzene–oxygen flame C/O = 0.8 with an unburned velocity of 42 cm s^{-1}, $p = 2.66$ kPa [18], and an acetylene/oxygen flame at a pressure of 2.67 kPa [19] have been experimentally studied by Homann et al. They measured PAH, PAH radicals, and PAH ions in these flames by means of resonant (REMPI) and nonresonant multiphoton ionization with a frequency-doubled, pulsed dye laser and separation with a time-of-flight mass spectrometer, equipped with an ion reflector. We use their experimental data to validate the AMPI code, treating the chemistry of the charged and uncharged PAH the same because of the similarity of their reactions, as discussed by Homann [20]. The concentrations of the gas-phase species that can contribute to the molecular growth of the aromatic compound have been calculated using the CHEMKIN package [21] together with a kinetic model previously developed [22]. In using these concentrations in the atomistic model, no allowance was made in the calculated hydrocarbons and H profiles for species depletion or temperature change.

The choice of the compounds that contribute to aromatic growth is based on their high concentrations

Table 1
Main reaction rate constants in the AMPI code

Species	Site for addition[a]	A[b]	n	E
H[c]	HCCCCCH	3.23E7	2.09	19,800.0
H[d]	SP^3 C	1.48E14	0.00	13,585.0
H[e]	*CCCCCCH	1.11E16	−0.82	690.0
H[f]	*CCCCCH	1.24E33	−5.68	8910.0
CH_3[f]	*CCCCCCH	3.05E52	11.80	17,660.0
CH_3[g]	Abstraction	1.20E13	0.00	5148.0
C_2H[h]	HCCCCCCH	1.00E12	0.00	0.0
C_2H_2[f]	*CCCCCH	1.12E26	−3.42	20,870.0
C_2H_2[f]	*CCCCCCH	8.56E44	−10.50	13,220.0
C_2H_3[f]	*CCCCCCH	1.75E49	−10.31	24,270.0
C_2H_3[i]	HCCCCCCH	7.94E11	0.00	6399.0
C_2H_4[i]	*CCCCCCH	1.99E13	0.00	0.0
C_2H_5[j]	Abstraction	1.20E13	0.00	5100.0
H_2CCCH[k]	*CCCCCCH	3.00E12	0.00	0.0
H_2CCCCH[l]	*CCCCCCH	6.00E12	0.00	0.0
HCCHCCH[f]	*CCCCCCH	1.84E72	−16.13	57,630.0
$CH_2CHCHCH$[m]	*CCCCCCH	2.80E–7	5.63	−1890.0
C_5H_6[n]	*CCCCCCH	1.00E–1	4.0	0.0
C_5H_5[o]	HCCCCCH	3.12E0	2.70	8860.0
C_5H_5[o]	*CCCCCH	1.89E–1	2.16	48.60
C_6H_6[p]	*CCCCCCH	1.90E76	−18.90	39,470.0
C_6H_6[g]	Abstraction	1.20E13	0.0	5148.0
C_6H_5[f]	*CCCCCCH	5.94E42	−8.83	13,830.0
C_6H_5[q]	HCCCCCCH	1.90E76	−18.90	39,470
C_6H_5[o]	HCCCCCH	2.43E1	3.04	2320.0
Indene[i]	*CCCCCCH	2.51E12	0.00	6200.0
Naphthalene[i]	*CCCCCCH	7.94E11	0.00	6399.0
1*Naphthyl[f]	*CCCCCCH	5.94E42	−8.83	13,830.0
1*Naphthyl[q]	*CCCCCH	12.93E0	3.62	183.12
2*Naphthyl[f]	*CCCCCCH	4.85E27	−4.32	6940.0
1*Naphthyl[p]	HCCCCCCH	1.90E76	−18.90	39,470.0
2*Naphthyl[p]	HCCCCCCH	1.90E76	−18.90	39,470.0
Acenaphthylene[q]	*CCCCCCH	12.93E0	3.62	183.12
3*Acenaphthyl[f]	*CCCCCCH	5.94E42	−8.83	13,830.0
3*Acenaphthyl[p]	HCCCCCCH	1.90E76	−18.90	39,470.0
4*Acenaphthyl[f]	*CCCCCCH	5.94E42	−8.83	13,830.0
4*Acenaphthyl[p]	HCCCCCCH	1.90E76	−18.90	39,470.0
5*Acenaphthyl[f]	*CCCCCCH	5.94E42	−8.83	13,830.0
5*Acenaphthyl[p]	HCCCCCCH	1.90E76	−18.90	39,470.0
Indenyl[f]	*CCCCCH	5.00E12	0.00	8000.0
Biphenyl[f]	*CCCCCCH	5.94E42	−8.83	13,830.0
Ring closure HCCCCC*=HCCCCC (ring formed)[o]		3.86E11	0.212	17,700.0

[a] Asterisks indicate sites on the growing aromatic where the addition reactions occur.
[b] Rate coefficients in the form $k = AT^n \cdot \exp(-E/RT)$. Units: mol, cm, s, K, and cal/mol.
[c] A.M. Mebel, M.C. Lin, T. Yu, K. Morokuma, J. Phys. Chem. A 101 (1997) 3189–3196.
[d] V.D. Knyazev, S.I. Stoliarov, I.R. Slagle, Proc. Combust. Inst. 26 (1996) 513–519.
[e] A.M. Mebel, M.C. Lin, D. Chakraborty, J. Park, S.H. Lin, Y.T. Lee, J. Chem. Phys. 114 (2001) 8421–8435.
[f] H. Richter, T.G. Benish, O.A. Mazyar, W.H. Green, J.B. Howard, Proc. Combust. Inst. 28 (2) (2000) 2609–2618.
[g] J.L. Emdee, K. Brezinsky, I. Glassman, J. Phys. Chem. 96 (1992) 2151–2161.
[h] M.B. Colket, Proc. Combust. Inst. 21 (1986) 851–864.
[i] A. Fahr, S.E. Stein, Proc. Combust. Inst. 22 (1988) 1023–1029.
[j] H.-Y. Zhang, J.T. McKinnon, Combust. Sci. Technol. 107 (1995) 261–300.
[k] A. D'Anna, A. Violi, Proc. Combust. Inst. 27 (1998) 425–433.
[l] C.J. Pope, J.A. Miller, Proc. Combust. Inst. 28 (2000) 1519–1527.
[m] P.R. Westmoreland, A.M. Dean, J.B. Howard J.P. Longwell, J. Phys. Chem. 93 (1989) 8171–8180.

Table 1 (*continued*)

[n] X. Zhong, J.W. Bozzelli, J. Phys. Chem. A 102 (1998) 3537–3555.
[o] A. Violi, et al. (2004), in preparation.
[p] J. Park, S. Burova, A.S. Rodgers, M.C. Lin, J. Phys. Chem. A 103 (1999) 9036–9041.
[q] A. Violi, T.N. Truong, A.F. Sarofim, Combust. Flame 126 (1/2) (2001) 1506–1515.

in the PAH inventory and to the important role played by PAH with peripherally fused five-membered rings (CP-PAH), which include acenaphthylene, in the formation of soot [15,23–28] and fullerenes [29]. Acetylene is the most abundant building block [30] and contributes to the HACA mechanism.

Having a diverse molecular base for the reaction sequence of hydrogen abstraction followed by addition to the radical site leads to a network of aromatic–aliphatic linked structures that have been identified in several experiments [31–34].

3. Results and discussion

3.1. H/C ratio

Keller et al. [18] report the molecular formulas of PAH in a C/H diagram for the benzene flame, where each point corresponds to a certain formula C_xH_y. The totality of points represents the ensemble of PAH and PAH radicals with different molecular formulas. The experimental data for the development of the ensemble of PAHs with up to 70 C atoms have been replotted in Fig. 1 as empty diamond points for the aromatic flame at distances of $h = 7$ and 10 mm above the burner.

The dashed line, provided for reference, corresponds to pericondensed polybenzenoid structures (benzene, pyrene, coronene, circumcoronene), the H/C of which is given by

$$\mathrm{H/C} = 1/n,$$

and the circular series index is

$$n = (C/6)^{0.5},$$

where C is the number of carbon atoms in the aromatic cluster [35]. The points above and below the line correspond to PAH that are H-rich and H-poor PAH relative to the most condensed six-ring structures.

In the same figure the filled diamonds represent the results, obtained through the use of the AMPI code, that match the experimental data from Homann, while the asterisks are the modeling results that do not have correspondence in experimental data. In the experiments, at a height above the burner of 7 mm (T around 1800 K) some PAH have grown to a C of 70 atoms, and the ensemble is composed mainly of

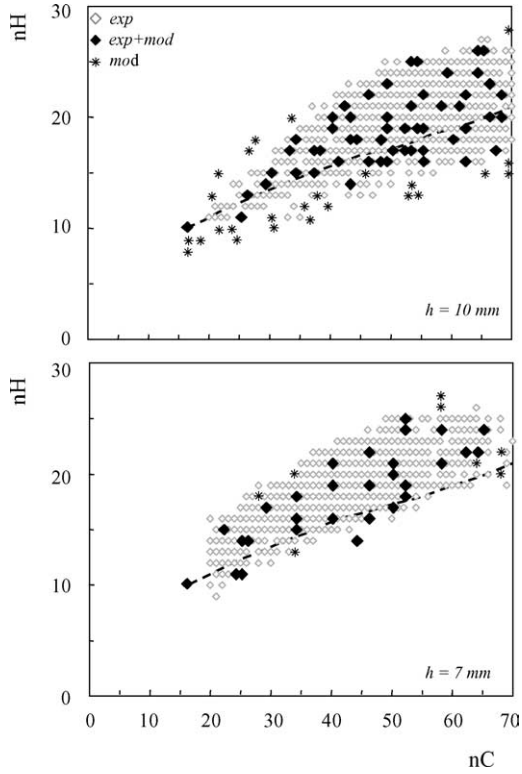

Fig. 1. C/H diagram of PAH and PAH radicals at different distances from the burner for the benzene flame. The dashed line marks maximum condensed six-ring PAH. Open diamonds, experimental data; filled diamonds, modeling results that match the experimental data; asterisks, modeling results.

H-rich species. At 10 mm (T around 2200 K) compounds with a larger number of carbons and compounds that are H-poor begin to appear. The computed structures are able to show this change. There are many reasons for a variation in the relative H content. Increases in H/C ratio result from (1) substituting hydrogen with a methyl, and (2) carbon structures more open than those found in aromers [18]. Decreases in H/C ratio result from (1) replacing a hydrogen with an ethynyl group, (2) incorporating five-membered rings into the structure, or (3) dehydrogenation reactions that lead to the loss of two hydrogens and ring closure. This implies that aromatics with the same number of carbon atoms, but different numbers of hydrogen atoms, may have very little in common in terms of structure and mechanisms of formation. Fig. 2 shows an example of the struc-

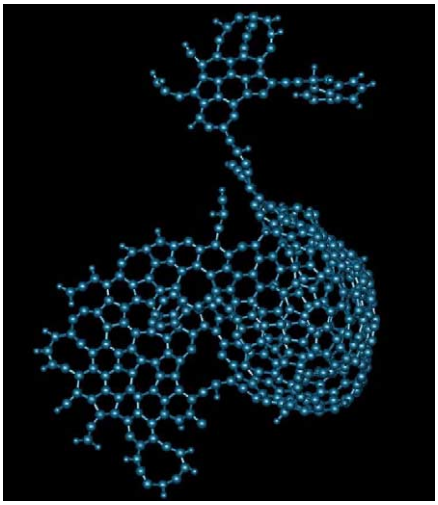

Fig. 2. Structure of a particle formed in benzene flame.

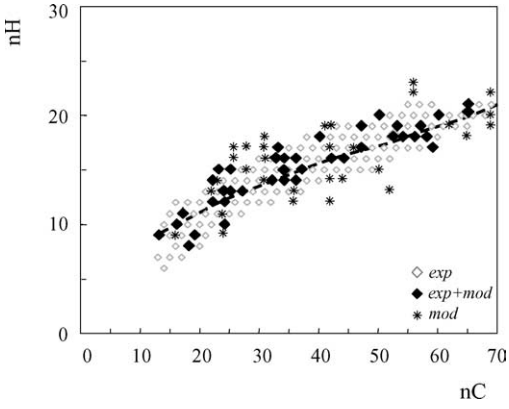

Fig. 3. C/H diagram for the acetylene flame. The dashed line marks maximum condensed six-ring PAH. Open diamonds, experimental data; filled diamonds, modeling results that match the experimental data; asterisks, modeling results.

tures computed for nanoparticles at $h = 10$ mm. The structure shows a high degree of curvature, as a consequence of dehydrogenation reactions and ring closure leading to five-membered rings. Presently, the model does not incorporate the oxidation reactions that can reduce the rate of growth.

The computed and measured H/C ratios of PAH fall in a broad band around the pericondensed benzenoid line due to the variance in H content for the same number of C atoms. This distribution widens as the number of carbon atoms increases. Fig. 3 shows the C/H diagram for molecular formulas of even- and odd-numbered PAH^+ with up to 70 C atoms for a low-pressure, fuel-rich, premixed acetylene/oxygen flame. The open diamonds are the experimental data obtained by Homann and co-workers [19], while the asterisks are the computed results, and the filled diamonds are the modeling results that match the experimental data.

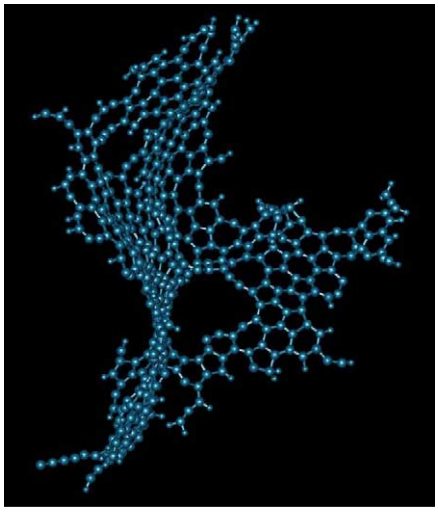

Fig. 4. Structure of a particle formed in acetylene flame.

The dominant PAH up to $C_{70}H_y$ in the acetylene flame are densely grouped around the pericondensed benzenoid line. The plotted C/H ratios form a staircase structure, with each step displaced to higher carbon and hydrogen atoms but having an approximately constant spam of H atoms. The band of growth follows the line of maximally condensed hexagons fairly well. Fig. 4 is an example of a computed structure produced in the acetylene environment. For comparison the structure presented in Fig. 4 has the same number of C atom as the structure shown in Fig. 2. Note that the particle formed in an acetylene environment has much less curvature than that produced in a benzene environment.

3.2. Aspect ratio

Another important characteristic of these particles is their morphology. Ellipticity parameters are often used to characterize particle shape [36]. To characterize ellipticity, the aspect ratio AR is defined as a/b, where a and b are the major and minor axes of the particle. A series of diameters of particles are sampled. The average of these diameters is used as the spherical diameter r_s of the particle, and the averages of the longest and shortest diameters are used as a and b, respectively. A better evaluation of a and b can be obtained using the Legendre ellipse, which has the same geometrical moments up to the second order as the original object area in this case, the projection of the particle in the a–b plane. The Legendre ellipse is often used instead of the original object. The aspect ratio of the particle, defined as a/b, is reported in Fig. 5 as a function of the equivolume diameter (ED)

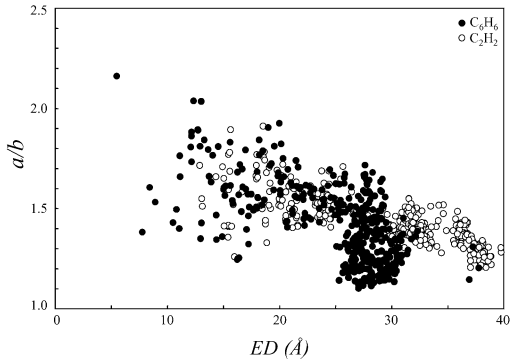

Fig. 5. Computed aspect ratios of soot precursor molecules as a function of equivalent spherical diameter in Ångstroms for the acetylene (open circles) and benzene (filled circles) flames.

calculated for a spherical particle encompassing the same volume.

4. Discussion

The gas-phase concentrations were computed using the Richter et al. [22] mechanism. For a benzene flame, with a C/O ratio of 0.8, the benzene concentration exceeds that of acetylene up to a height of about 8 mm ($T \approx 1900$ K). Higher in the flame, acetylene concentrations exceed those of benzene. As a consequence, the relative contributions to growth of the soot precursors change as combustion progresses, with benzene dominating early in the flame and acetylene and its derivatives dominating at later stages of combustion. This is illustrated in Table 2.

The percentage of carbon growth contributed by benzene decreases from 84% at a flame height of 7 mm to 13.1% at 10 mm. Allowance is made for the change in the gas-phase concentrations at different heights in calculating the soot precursor composition, but the depletion in gas-phase species by the formation of precursors is neglected.

Dehydrogenation reactions, which involve the loss of hydrogen with rearrangement of the structure to form new rings, are 11% of the reactions that occur at 1800 K, and their contributions increase to 22% at 2200 K. Within the oxidation zone the temperature rises and the number of vibrational degrees of freedom of the PAH increases with growth, factors that favor unimolecular reactions of PAH that normally have larger activation energies than addition reactions with unsaturated hydrocarbons. Unimolecular reactions of large PAH lead to structures that are more reactive to addition of smaller unsaturated hydrocarbons [18]. The larger the activation energy, the more rapidly the rates of elementary reactions increase with temperature. There is a competition between bimolecular association reactions (addition or growth reactions) and rearrangement reactions which exhibit higher activation energies: at the low temperatures at the beginning of the oxidation zone, the molecules grow but rearrangement and degradation reactions do not play a significant role [18]. With increasing temperature the growth reactions become faster but the rates of rearrangements increase even more rapidly. Cage closure reactions, breaking C–H bonds, and intramolecular rearrangements have large activation energies and are therefore favored at higher temperature.

Table 2
Flame properties and contribution of some species to the carbon growth

Flame height (mm)	7	10
Temperature (K)	1800	2130
C_2H_2	9E−6	4E−7
C_6H_6	6E−7	1E−9
	% C growth	
C_2H_2	6	35.0
C_6H_6	84	13.1
C_3H_3		26
CH_3	0.4	16.7
$C_{12}H_8$	9	6.6
C_2H_3	0.6	2.6

In contrast to the structures formed in the aromatic flame that show three-dimensional characteristics, the structures formed in the aliphatic flame are instead mainly planar and the contribution of acetylene is significant. This is in agreement with the finding reported by Homann et al. [19] that in an acetylene flame, high-mass PAH are essentially planar molecules. As the mass increases, the average C/H becomes lower than that of benzenoid PAH, hence slightly more rich in hydrogen.

The present results are also consistent with the polarization of light scattered by young soots. Haynes et al. [37] investigated soot formation in premixed flat flames of ethylene and benzene with air using laser light scattering and fluorescence and extinction measurements. They found that the depolarization of the light scattered (ρ_V) from the particles is of the order of 1% for ethylene and 0.2% for benzene flames. Furthermore, they observed that the depolarization ratio decreases with increasing height in the flame. These observations are qualitatively explained by the results above that show that the anisotropy of soot precursors is higher in acetylene than benzene flames and decreases with progress of reaction. The distinction is between aliphatic flames, in which the major growth species are acetylene and its derivatives, and aromatic flames, in which benzene or PAH additions dominate in the early stages of combustion.

5. Conclusions

The AMPI code provides a tool for studying in a chemically specific way the transformations that occur during the formation of soot precursors. The use of this methodology allows the study of long time scales, where the time between Monte Carlo events can be arbitrarily long (depending on the kinetics, model, etc.), whereas MD simulations require time steps that are a small fraction of the atomic vibrational period. The knowledge of the structures of soot precursors, obtained by applying the AMPI code to follow the time evolution of a statistical ensemble of molecules, can supply valuable guidance to the development of soot formation models.

The potential of the AMPI method is apparent from its ability to reproduce the H/C trends identified in aromatic and aliphatic flames. The reaction pathways for the growth of incipient soot particles seem to depend on the fuel. In the case of aromatic fuels, polymerization reactions can occur early, because aromatic compounds are in relatively large concentrations in the fuel, whereas in the case of aliphatic fuels such as acetylene, ethylene, and methane the first aromatic ring must be formed from fuel decomposition products by a sequence of elementary reactions and, therefore, the aromatic soot precursors are present in lower concentrations than in the aromatic flames. Hydrogen-poor PAH are formed primarily in acetylene flames up to about C100 PAH. In aromatic flames, fewer H-poor PAH are formed, whereas there are a significant number of H-rich PAH.

The use of this approach has also shown promise for explaining other properties such as particle morphology and depolarization ratio.

Acknowledgments

This research is funded by the University of Utah Center for the Simulation of Accidental Fires and Explosions (C-SAFE), funded by the Department of Energy, Lawrence Livermore National Laboratory, under Subcontract B341493 and by a National Science Foundation Nanoscale Interdisciplinary Research Team grant (EEC-0304433). The author wishes to acknowledge Dr. A. Kubota of Lawrence Livermore National Laboratory for her collaboration during the initial phases of the computer code development for his project. The calculations presented in this article were carried out at the Utah Center for High Performance Computing, University of Utah, which is acknowledged for computer time support.

References

[1] R.A. Dobbins, in: F.L. Dryer, R.F. Sawyer (Eds.), Combustion Science and Technology Book Series (Physical and Chemical Aspects of Combustion), Gordon & Breach, New York, 1997, p. 107.
[2] A. Violi, A. Kubota, T.N. Truong, W.J. Pitz, C.K. Westbrook, A.F. Sarofim, Proc. Combust. Inst. 29 (2002) 2343–2349.
[3] A. Violi, G.A. Voth, A.F. Sarofim, Combust. Sci. Technol. 176 (2004) 991–1005.
[4] A.B. Bortz, M.H. Kalos, J.L. Lebowitz, J. Comp. Phys. 17 (1975) 10–18.
[5] A.F. Voter, Phys. Rev. B 34 (1986) 6819–6829.
[6] K.A. Fichthorn, W.H. Weinberg, J. Chem. Phys. 95 (1991) 1090–1096.
[7] C.C. Battaile, D.J. Srolovitz, J.E. Butler, J. Appl. Phys. 82 (1997) 6293–6300.
[8] A. Violi, A. Kubota, W.J. Pitz, C.K. Westbrook, A.F. Sarofim, Prepr. Symp. Am. Chem. Soc. Div. Fuel Chem. 47 (2002) 771–772.
[9] S.J. Stuart, A.B. Tutein, J.A. Harrison, J. Chem. Phys. 112 (2000) 6472–6486.
[10] A. D'Anna, A. Violi, Proc. Combust. Inst. 27 (1998) 425–433.
[11] M. Frenklach, S. Taki, M.B. Durgaprasad, R.A. Matula, Combust. Flame 54 (1983) 81–101.
[12] M. Frenklach, D.W. Clary, W.C. Gardiner Jr., S.E. Stein, Proc. Combust. Inst. 20 (1985) 887–901.
[13] H. Wang, M. Frenklach, Combust. Flame 110 (1997) 173–221.
[14] M. Frenklach, J. Warnatz, Combust. Sci. Technol. 51 (1987) 265–283.
[15] A. Violi, A.F. Sarofim, T.N. Truong, Combust. Flame 126 (2001) 1506–1515.
[16] M. Frenklach, H. Wang, Proc. Combust. Inst. 23 (1991) 1559–1566.
[17] H. Richter, O.A. Mazyar, R. Sumathi, W.H. Green, J.B. Howard, J.W. Bozzelli, J. Phys. Chem. A 105 (2001) 1561–1573.
[18] A. Keller, R. Kovacs, K.-H. Homann, Phys. Chem. Chem. Phys. 2 (2000) 1667–1675.
[19] P. Weilmunster, A. Keller, K.-H. Homann, Combust. Flame 116 (1999) 62–83.
[20] K.-H. Homann, Angew. Chem. Int. Ed. 37 (1998) 2434–2451.
[21] R.J. Kee, F.M. Rupley, J.A. Miller, Chemkin II: A Fortran Chemical Kinetics Package for the Analysis of Gas Phase Chemical Kinetics, Report No. SAND 89-8009B, Sandia National Laboratories, 1989.
[22] H. Richter, T.G. Benish, O.A. Mazyar, W.H. Green, J.B. Howard, Proc. Combust. Inst. 28 (2000) 2609–2618.
[23] T.G. Benish, A.L. Lafleur, K. Taghizadeh, J.B. Howard, Proc. Combust. Inst. 26 (1996) 2319–2326.
[24] C.S. McEnally, L.D. Pfefferle, Combust. Sci. Technol. 131 (1998) 323–344.
[25] M. Frenklach, L.B. Ebert, J. Phys. Chem. 92 (2) (1988) 561–563.
[26] M. Frenklach, N.W. Moriarty, N.J. Brown, Proc. Combust. Inst. 27 (1998) 1655–1661.
[27] M. Frenklach, Proc. Combust. Inst. 26 (1996) 2285–2293.

[28] J.A. Mulholland, M. Lu, D.-H. Kim, Proc. Combust. Inst. 28 (2000) 2593–2599.
[29] A.L. Lafleur, J.B. Howard, K. Taghizadeh, E.F. Plummer, L.T. Scott, A. Necula, K.C. Swallow, J. Phys. Chem. 100 (1996) 17,421–17,428.
[30] M. Frenklach, Phys. Chem. Chem. Phys. 4 (2002) 2028–2037.
[31] A. D'Alessio, A. D'Anna, A. D'Orsi, P. Minutolo, R. Barbella, A. Ciajolo, Proc. Combust. Inst. 24 (1992) 973–980.
[32] A. Ciajolo, R. Barbella, A. Tregrossi, L. Bonfanti, Proc. Combust. Inst. 27 (1998) 1481–1487.
[33] R.A. Dobbins, H. Subramaniasivam, in: H. Bockhorn (Ed.), Soot Formation in Combustion, Springer-Verlag, Heidelberg, 1994, p. 290.
[34] R.A. Dobbins, R.A. Fletcher, H.-C. Chang, Combust. Flame 115 (1998) 285–298.
[35] M.S. Solum, R.J. Pugmire, D.M. Grant, Energy Fuels 3 (1989) 187–193.
[36] V. Mikli, H. Kaerdi, P. Kulu, M. Besterci, Proc. Estonian Acad. Sci. Eng. 7 (2001) 22–25.
[37] B.S. Haynes, H. Jander, H.Gg. Wagner, Ber. Bunsenges. Phys. Chem. 84 (1980) 585–592.